

## ARTICLE OPEN



# TSPYL5-driven G3BP1 nuclear membrane translocation facilitates p53 cytoplasm sequestration via accelerating RanBP2-mediated p53 sumoylation and nuclear export in neuroblastoma

Zhaokun Wang<sup>1,2</sup>, Yunqiang Liu<sup>1,2</sup>, Yangwei Zhang<sup>1,2</sup>, Jiaying Shi<sup>1</sup>, Shengyu Xie<sup>1</sup>, Ming Yi<sup>1</sup>, Xinyue Zhang<sup>1</sup>, Dachang Tao<sup>1</sup> and Yuan Yang<sup>1</sup>

© The Author(s) 2025

Cytoplasmic sequestration of wild-type p53, representing a nonmutational event of p53 activity suppression, is a characteristic phenotype of undifferentiated neuroblastoma (NB); however, the underlying mechanism is yet to be defined. In the present study, we observed that TSPYL5 effectively tethers p53 in the cytoplasm and greatly inhibits its function as a transcription factor. Mechanistically, the binding of TSPYL5 with G3BP1 enhances G3BP1 Ser149 phosphorylation to drive G3BP1 nuclear membrane translocation, which recruits more p53 for nucleoporin RanBP2 by the formation of the RanBP2-G3BP1-p53 complex. Thus, the accelerating p53 sumoylation promotes its nuclear export. With this signal pathway, TSPYL5 augments the malignant characteristics of neuroblastoma cells. Our findings unravel a detailed TSPYL5-driven molecular axis that sheds light on the regulating system of the p53 sumoylation-based cytoplasmic sequestration in NB cells, paving the way for the novel therapeutic opportunities for NB cancers by antagonizing TSPYL5 function.

*Cell Death and Disease* (2025)16:358; <https://doi.org/10.1038/s41419-025-07694-x>

## INTRODUCTION

Neuroblastoma (NB), the most common cause of cancer-related death in childhood, is responsible for ~15% of pediatric cancer deaths [1]. NB commonly originates from the undifferentiated neural crest cells during fetal development and about 65% of NB specimens were examined to possess the characteristics of cancer stem cells (CSCs) such as chemoradiotherapy resistance and distant metastasis [2]. It is well known that the tumor suppressor p53 plays crucial roles in the cellular processes including self-renewal, differentiation, and reprogramming of stem cells [3], and loss of p53 has been demonstrated to account for CSCs amplification in some tumors [4, 5]. p53 is rarely mutated in neuroblastoma, however, the cytoplasmic sequestration of wild-type p53, which is proposed as a non-mutational mechanism for p53 inactivation, is present in about 95% of undifferentiated NB cases [6]. Thus, it is greatly possible that the p53 cytoplasmic sequestration dramatically reduces p53 transcriptional activity and then increases the CSC amount of NB, contributing to poor prognosis of NB patients. Indeed, reactivating wild-type p53 has been suggested as a promising strategy to improve NB therapy [7]. Before that, however, the mechanism underlying the cytoplasmic p53 sequestration needs to be intensively examined in NB.

Several mechanisms have been proposed for cytoplasmic p53 sequestration. It is frequently observed that the C-terminal domain of p53 is anchored by other proteins or long noncoding RNAs [8, 9], forming a large protein aggregate to tether p53 in the cytoplasm. Another more common and efficient factor responsible for p53 cytoplasm localization is the ubiquitylation status in its C-terminus, in which monoubiquitination facilitates nuclear export [10], and recent report further suggests that the SUMO modification of monoubiquitinated p53 promotes its cytoplasmic translocation [11]. However, the regulators driving and controlling the p53 posttranslational modification (PTM)-mediated cytoplasmic accumulation are still not well understood.

TSPYL5 (TSPYL5), an autosome-encoded homologous protein of testis-specific protein Y-linked 1 (TSPY1), is variably expressed in human tissues and mainly in the testis. Additionally, TSPYL5 has also been reported to be abundantly expressed in many adult tumors, correlated with their poor progression [12–14]. As a conserved C-terminal nucleosome assembly protein, TSPYL5 is expected to play roles in chromosome assembly, histone replacement, tissue-specific gene transcriptional regulation, and cell cycle regulation. Notably, TSPYL5 interacts with USP7 (ubiquitin specific peptidase 7) to reduce the tumor suppressor activity of p53, overriding p53-dependent proliferation arrest [12],

<sup>1</sup>Department of Medical Genetics, State Key Laboratory of Biotherapy, West China Hospital, Sichuan University, Chengdu, China. <sup>2</sup>These authors contributed equally: Zhaokun Wang, Yunqiang Liu, Yangwei Zhang. ✉email: yangyuan@scu.edu.cn  
Edited by Dr Angelo Peschiaroli.

Received: 5 August 2024 Revised: 7 April 2025 Accepted: 24 April 2025  
Published online: 03 May 2025

promoting endothelial cell proliferation and angiogenesis [15], and protecting POT1 (protection of telomeres 1) from proteasomal degradation in ALT (alternative lengthening of telomeres)-positive cells [16]. Additionally, TSPYL5 has been demonstrated to be critical for maintaining CSC-like characteristics of cancer cells [13]. Importantly, our recent investigation suggested that the high expression of TSPYL5 effects the cytoplasmic p53 sequestration and transcriptional inactivity in NB cells, providing an opportunity to shed light on the mechanism underlying the cytoplasmic sequestration of p53 by exploring the role of TSPYL5 in regulating p53 nucleocytoplasmic transport in NB tumors.

In this study, we unveils the regulation mechanism underlying the cytoplasmic p53 sequestration of NB cells, by which TSPYL5 drives G3BP1 (G3BP stress granule assembly factor 1)/RanBP2 (RAN binding protein 2)/SUMO (small ubiquitin-related modifier)-mediated p53 sumoylation, enhancing p53 nuclear export signal and inhibiting its tumor suppressor activity.

## RESULTS

### TSPYL5 augments the malignant characteristics of NB cells by suppressing the transcriptional activity of p53

We firstly found that the high expression of *TSPYL5* in NB tumors and cells (Supplementary Fig. 1a, b), and the single-cell transcriptomes of NB tissues further demonstrated its specific expression in neuroendocrine (NE) cells (Supplementary Fig. 1c–f), the representative malignant cells of NB tumors [17]. To investigate the role of *TSPYL5* in NB tumors, we selected two regularly used cell lines in NB studies, including SK-N-SH and SH-SY5Y. After confirming that *TSPYL5* was abundantly expressed in the cytoplasm (Supplementary Fig. 2a), we established the *TSPYL5*-knockdown models of the two cell lines (Supplementary Fig. 2b). Then, we explored the potential function of *TSPYL5* by RNA-seq of the two models. As a result, more than 14,000 DEGs were observed in both cell lines with similar gene expression patterns (GSE223866) (Supplementary Fig. 3a, b). Even if the filtering threshold was been set to  $|\log_2\text{fold change}| > 2$  and  $\text{Padj} < 0.05$ , 5763 and 5880 DEGs were identified in SK-N-SH and SH-SY5Y, respectively. Interestingly, the p53 signaling pathway was enriched via both KEGG and Reactome analysis of SK-N-SH DEGs and the similar result obtained also in RNA-seq analysis of SH-SY5Y cells (Fig. 1A, B). Several cell functions associated with the p53 signaling pathway, including DNA replication, RNA splicing, and intercellular adhesion [18–20], were also enriched via GO analysis (Supplementary Fig. 3c).

It is well known that p53 functions as a transcription factor to suppress the malignant transformation of cells [21]. For this, our transcriptome data were further excavated to determine the DEGs involved in the p53 signaling pathway. As a result, a total of 17 p53-related genes were confirmed to be remarkably differentially expressed in both NB cell lines ( $|\log_2\text{fold change}| > 2$ ,  $\text{Padj} < 0.05$ ) (Fig. 1C), totally suggesting the upregulation of p53 function in *TSPYL5*-knocked down NB cells (Fig. 1D). Then, we extracted the data from TARGET (<https://ocg.cancer.gov/programs/target>) to examine the correlation between the expression of *TSPYL5* and these p53-targeted DEGs in NB tissues. The results showed that the correlations between the expression of *TSPYL5* and ten p53-targeted genes, including *SERPINE1*, *THBS1*, *FAS*, *CD82*, *CASP8*, *CASP9*, *BBC3*, *DRAM1*, *SHISA5*, and *GADD45B*, were consistent with those from our transcriptomic analysis (Supplementary Fig. 4a–j). For each of seven p53-directly targeted genes, including *SERPINE1*, *SHISA5*, *BAX*, *FAS*, *CDKN1A*, *RRM2* and *DRAM1*, the significantly upregulated expression in both *TSPYL5*-knockdown SK-N-SH and SH-SY5Y cells was further confirmed (Fig. 1E). In addition, reanalysis of the single-cell transcriptome further demonstrated a negative regulation of *TSPYL5* on the p53 signaling pathway (Supplementary Fig. 3d). These findings suggest that *TSPYL5* effectively suppresses p53 transcriptional activity in NB cells.

Among these p53-related DEGs, *SERPINE1*, *CD82* and *THBS1* inhibit metastasis, invasion and angiogenesis of tumor cells [22], *SHISA5*, *ZMAT3*, *FAS*, *TNFRSF10B*, *CASP8*, *CASP9*, *BAX*, *BBC3*, and *BCL2* promote cell apoptosis and increase sensitivity to drug [23], *FAS* and *TNFRSF10B* have also been reported to support CSC maintenance [24], *CDKN1A*, *RRM2*, *GADD45B*, and *RRM2B* mediate cell cycle arrest [25], and *DRAM1*, *RRM2*, and *RRM2B* are also required for the repair of DNA damage [26]. To investigate whether the suppression of p53 activity by *TSPYL5* observably affects the functions of NB cells, we examined the p53-related cell phenotypes, including cell proliferation, apoptosis, clonal and sphere formation, side population ratio, invasiveness, and migration of NB cells with different levels of *TSPYL5*. The results showed that the decrease in *TSPYL5* seriously reduced the viability and increased the apoptosis of NB cells treated with cisplatin, a commonly used chemotherapeutic agent, and the rescue of *TSPYL5* expression restored the proliferation and inhibited the apoptosis of cisplatin-treated NB cells (Fig. 2A, B). Additionally, the knockdown of *TSPYL5* significantly reduced the number of cell colonies and the size of sphere as well as the ratio of side population cells (Fig. 2C–E), clearly inhibited the invasiveness and migration of NB cells (Fig. 2F, G) and while the exogenous expression of *TSPYL5* rescued the above phenotypes (Fig. 2C–G). These observations suggest that the knockdown of *TSPYL5* expression contributes to the inhibition of NB malignant progression via activating the p53 tumor suppressor.

In order to investigate whether *TSPYL5*'s impacts on NB malignant progression are dependent on p53 activity, we reduced the p53 expression in the *TSPYL5*-knockdown NB cells using the *TP53*-targeted siRNA (Supplementary Fig. 5a, b). We found that the downregulated p53 expression significantly decreased its targeted genes expression which had been augmented in the *TSPYL5*-knockdown NB cells (Supplementary Fig. 5c). Furthermore, we observed that the p53 decreasing enhanced the viability and reduced the apoptosis of the *TSPYL5*-knockdown NB cells treated with cisplatin (Supplementary Fig. 6a, b). Additionally, further reducing the p53 expression in the *TSPYL5*-knockdown NB cells obviously increased the number of cell colonies and the size of sphere as well as the ratio of side population cells (Supplementary Fig. 6c–e), and also enhanced the invasiveness and migration capacity (Supplementary Fig. 6f, g). Taken together, these results further supported that *TSPYL5* augments the malignant characteristics of NB cells through regulating the p53 signaling pathway.

### TSPYL5 effects cytoplasmic p53 sequestration by promoting SUMO-mediated nuclear export

In NB cells, the inhibition of p53 function by *TSPYL5* was not due to a decrease in the mRNA and protein levels of p53 (Fig. 3A). In this case, our first idea was whether *TSPYL5* could regulate p53 subcellular localization. Indeed, previous studies have reported the cytoplasmic sequestration of wild-type p53 in undifferentiated NB tumors [27]. In the present study, we found that p53 was mainly located in the cytoplasm of SK-N-SH and SH-SY5Y cells, while it was redistributed in the nucleus of *TSPYL5*-knockdown cells, and the rescue of *TSPYL5* expression restored cytoplasmic p53 localization (Fig. 3B). This observation was confirmed by the nucleus-plasm separation experiment (Fig. 3C, Supplementary Fig. 7a, b). These results suggest that *TSPYL5* suppresses the transcriptional activity of p53 by facilitating cytoplasmic p53 sequestration in NB cells.

The PTMs of p53 have been suggested to determine the subcellular localization of p53 [10, 11]. In this case, we compared the degree of p53 ubiquitination among NB cells with different *TSPYL5* expression levels. Impressively, we observed a high level of monoubiquitinated, not polyubiquitinated, p53 in NB cells and found that the monoubiquitination of p53 was enhanced with increasing *TSPYL5* expression (Fig. 3D). Previous studies have

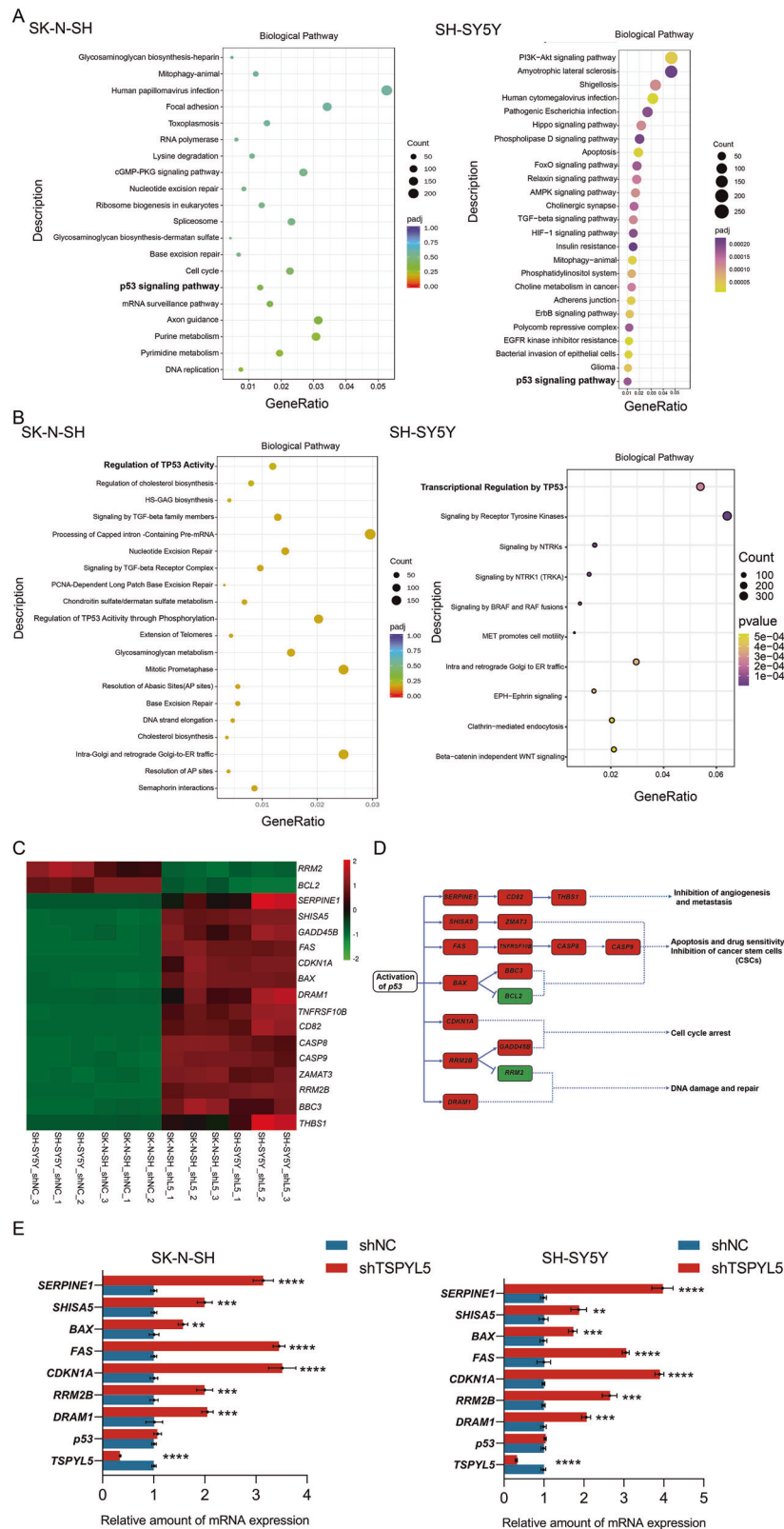


**Fig. 1** TSPYL5 inhibits p53-mediated transcriptional activity. **A** KEGG enrichment analysis of the differentially expressional genes (DEGs) observed in the RNA-seq of SK-N-SH and SH-SY5Y cells transfected with shNC and shTSPYL5. **B** Reactome enrichment analysis of DEGs of the TSPYL5-knocked down SK-N-SH and SH-SY5Y cells. **C** Heatmap of the 17 DEGs involved in the p53 signaling pathway in the SK-N-SH and SH-SY5Y cells. The unit for the color scale was the z score of  $\log_2$  expression data shown on the right side of the diagram. **D** The location of the p53-related DEGs in the p53 signaling pathway as annotated by KEGG. The names of upregulated DEGs in the TSPYL5-knocked down cells were covered in red and those of downregulated DEGs were covered in green. The functions of the DEGs were shown in the right side of the diagram. **E** The validation analysis of the expression of seven p53-directly targeted genes in the SK-N-SH and SH-SY5Y transfected with shNC and shTSPYL5. The mean  $\pm$  SD from three experiments was plotted. \* $p < 0.05$ , \*\* $p < 0.01$ , \*\*\* $p < 0.001$ .

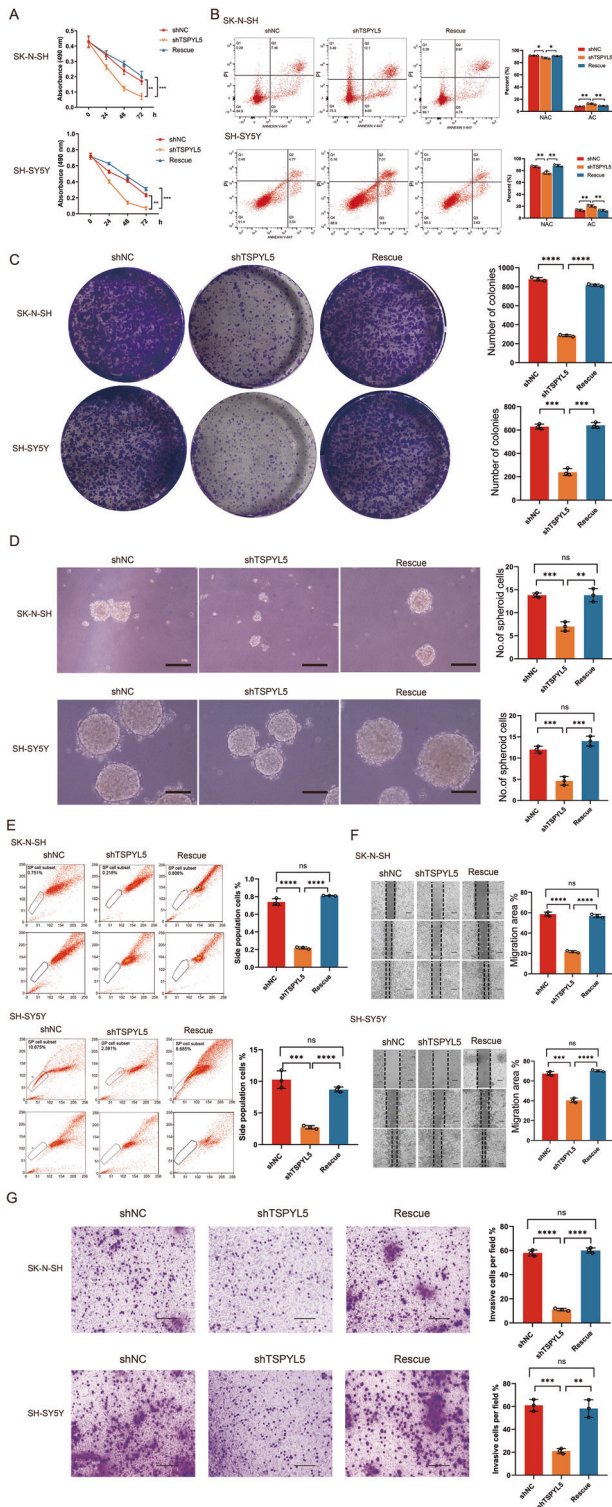


**Fig. 2 TSPYL5 augments the malignant characteristics of NB cells.**

**A** CCK-8 assays showing the sensitivity to cisplatin in the SK-N-SH and SH-SY5Y cells transfected with shNC or shTSPYL5. **B** Flow cytometry assays showing the apoptosis induced by cisplatin in the SK-N-SH and SH-SY5Y cells transfected with shNC and shTSPYL5. **C** Colony formation assays in the SK-N-SH and SH-SY5Y cells transfected with shNC or shTSPYL5. **D** Sphere formation assays in the SK-N-SH and SH-SY5Y cells transfected with shNC or shTSPYL5. Scale bar = 25  $\mu$ m. **E** Side population ratio assays in the SK-N-SH and SH-SY5Y cells transfected with shNC and shTSPYL5. **F, G** Migration and invasion assays in the SK-N-SH and SH-SY5Y cells transfected with shNC and shTSPYL5. Scale bar = 50  $\mu$ m. Rescue assays were used to exclude the off-target effect. ns = no significant difference. The mean  $\pm$  SD from three experiments was plotted. \* $p < 0.05$ , \*\* $p < 0.01$ , \*\*\* $p < 0.001$ .

MDM2 (Supplementary Fig. 8b). All of these results imply that under the unique molecular environment of low MDM2 levels, the high level of monoubiquitinated p53 in NB cells overexpressing TSPYL5 prepares for its nuclear export.

Monoubiquitinated p53 can be sumoylated, and p53 sumoylation can accelerate its nuclear export and cytoplasmic localization [10, 29]. It is reasonable, therefore, to presume that a considerable amount of cytoplasmic p53 may be SUMO-modified in NB cells. To test this hypothesis, we performed IP experiments of sumoylated p53 in both SK-N-SH and SH-SY5Y cells, and the results clearly showed an increase in sumoylated p53 when TSPYL5 was overexpressed (Fig. 3E). Then, using HA-tagged SUMO1 and Myc-tagged p53, we confirmed an enhanced interaction between SUMO1 and p53 in cells overexpressing TSPYL5 (Fig. 3F). Furthermore, we constructed a vector expressing p53 harboring K386R, a missense mutation inhibiting p53 sumoylation [30]. In H1299 cells lacking endogenous p53, we observed an upregulated sumoylation level of exogenous wild-type p53 when overexpressing TSPYL5, while such a role was not found in H1299 cells expressing exogenous p53-K386R (Fig. 3G), further supporting the promotion of p53 sumoylation by TSPYL5. All of these results suggest that TSPYL5 expression facilitates cytoplasmic p53 sequestration by enhancing p53 sumoylation-mediated nuclear export in NB cells. Additionally, a previous study reported the contribution of aberrant p53 hyperubiquitylation to cytoplasmic p53 sequestration in NB [31]. Actually, the ubiquitylated p53 in the report is almost monoubiquitylated. Overall, we speculate that the extremely low level of polyubiquitination prolongs the half-life of wild-type p53 so that a great amount of monoubiquitinated/sumoylated p53 accumulates in the cytoplasm of NB cells.

### TSPYL5-mediated p53 sumoylation depends on its interaction with G3BP1

To explore the mechanism underlying the promotion of p53 sumoylation by TSPYL5, we first investigated the function of the top 50 DEGs obtained from the RNA-seq analysis of the TSPYL5-knockdown cells, but we did not find any gene reported to be involved in p53 sumoylation (Supplementary Tables 4 and 5). Then, the TSPYL5-interacting proteins were investigated in NB cells by Co-IP following LC-MS/MS analysis. Consequently, G3BP1, a high-scoring partner of TSPYL5 (Fig. 4A), caught our attention since the protein has been suggested to promote cytoplasmic p53 localization [32], although the underlying mechanism was not associated with p53 modification. The following IP and western blotting analysis confirmed the binding between G3BP1 and TSPYL5 (Fig. 4B, C), which was supported by the computational docking model of the two molecules (Fig. 4D). The G3BP1 peptide from 200 aa to 330 aa containing the PXXP domain was further identified to be necessary for its interaction with TSPYL5 (Fig. 4E).

demonstrated that high levels of MDM2 (MDM2 proto-oncogene) are commonly required for p53 polyubiquitination and degradation, while low levels of MDM2 help the attachment of a single ubiquitin to the C-terminal lysines of p53 to initiate other modifications of monoubiquitinated p53 and nuclear export [10, 28]. Indeed, we observed that SK-N-SH and SH-SY5Y cells presented a lower level of MDM2 than other cells reported to possess a high level of MDM2 expression (Supplementary Fig. 8a) and that TSPYL5 could not obviously change the status of low

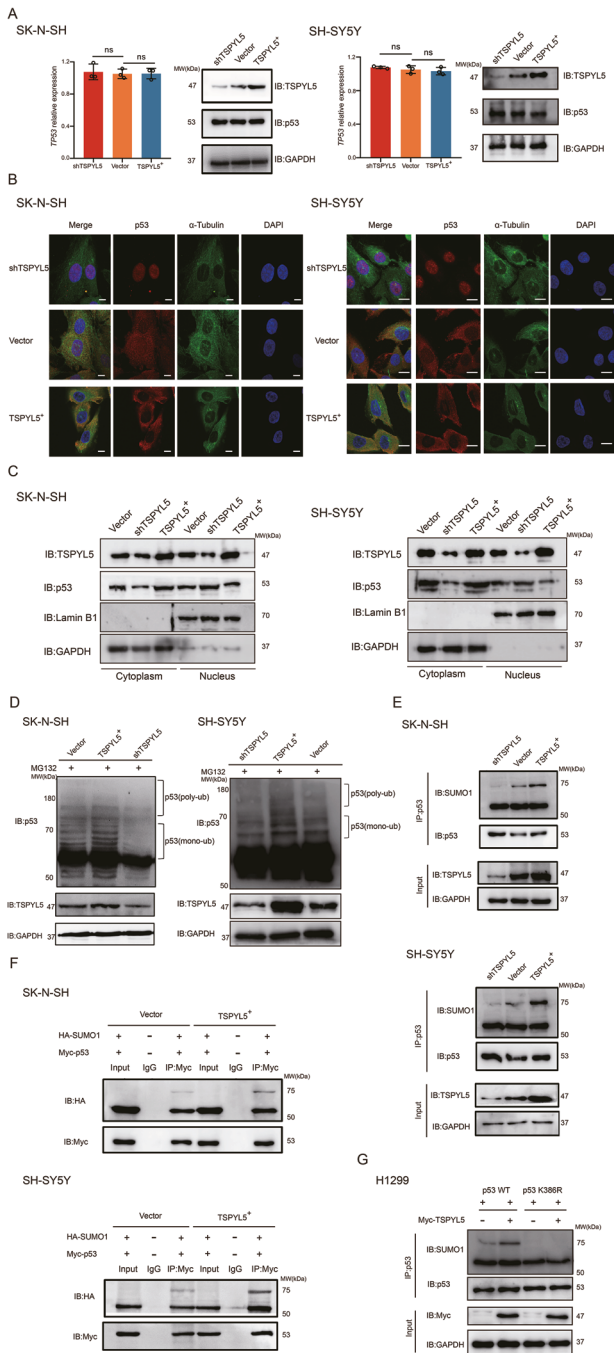


**Fig. 3 TSPYL5 enhances p53 cytoplasm sequestration by promoting p53 sumoylation.** **A** The comparison of p53 expression in the SK-N-SH and SH-SY5Y with different TSPYL5 expression level. ns no significant difference. **B** The comparison of p53 subcellular localization in the SK-N-SH and SH-SY5Y with different TSPYL5 expression level by immunofluorescence analysis. Cell nuclei were counterstained with 4,6-diamidino-2-phenylindole (DAPI). Scale bar = 10  $\mu$ m. **C** The comparison of p53 subcellular localization in the SK-N-SH and SH-SY5Y with different TSPYL5 expression level by the nucleus-plasm separation experiment. **D** The ubiquitination pattern of p53 in the SK-N-SH and SH-SY5Y cells with different TSPYL5 expression level. **E** The comparison of the level of SUMO1 immunoprecipitated with p53 in the SK-N-SH and SH-SY5Y cells with different TSPYL5 expression level. **F** The comparison of the level of exogenous HA-SUMO1 immunoprecipitated with Myc-p53 in the SK-N-SH and SH-SY5Y with different TSPYL5 expression level. **G** The comparison of the level of SUMO1 immunoprecipitated with exogenous Flag-p53 (wild-type) and Flag-p53 (K386R) in the H1299 with and without exogenous Myc-TSPYL5 expression.

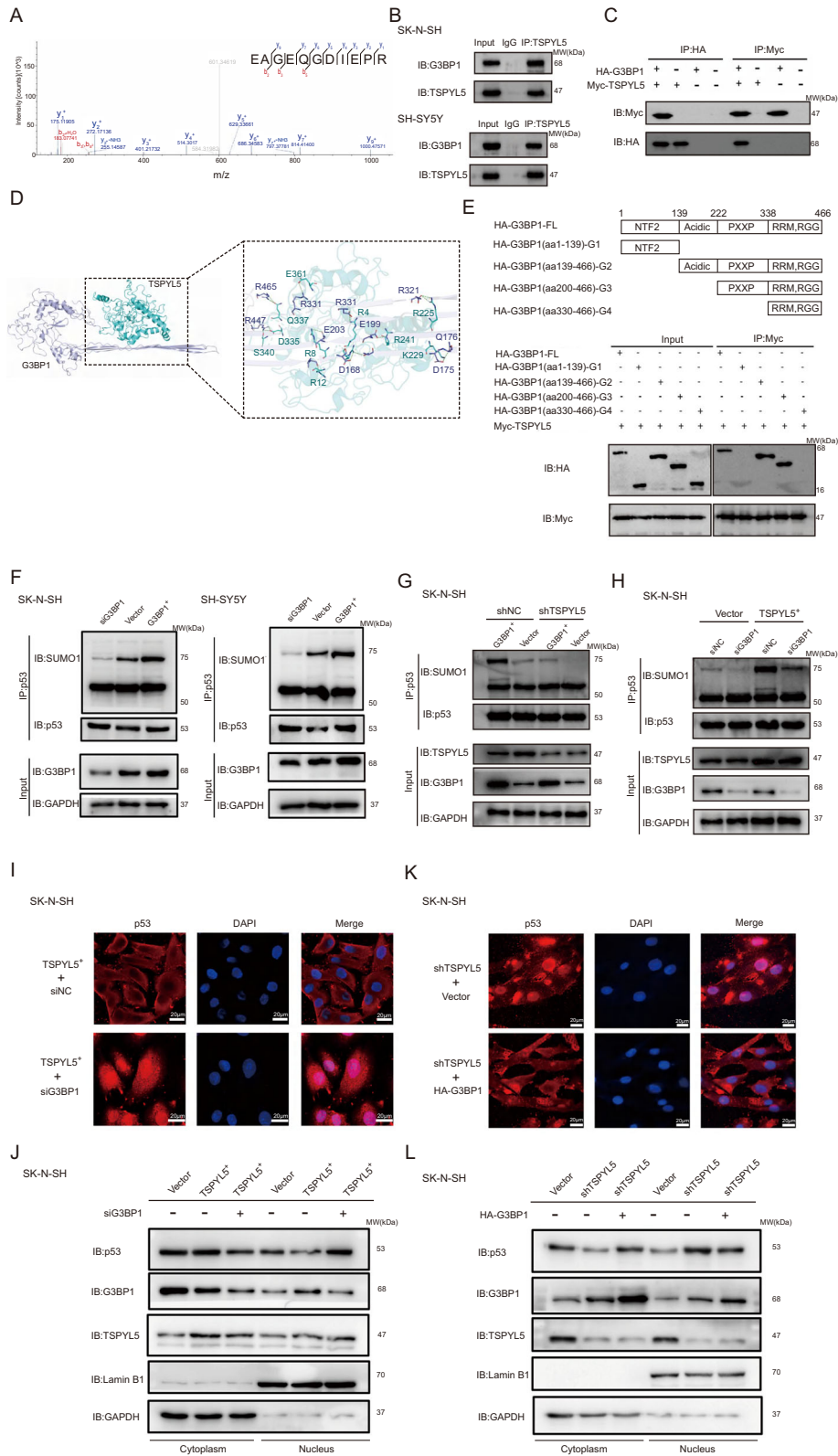
Furthermore, we found that G3BP1 increased the sumoylation of p53 in NB cells (Fig. 4F). Therefore, it is possible that the promotion of TSPYL5 on sumoylation and cytoplasmic localization of p53 is dependent on its interaction with G3BP1. To prove this idea, we performed IP experiments of sumoylated p53 in both SK-N-SH and SH-SY5Y cells with different levels of TSPYL5 and G3BP1. We clearly observed a dependence of TSPYL5-mediated p53 sumoylation on G3BP1 (Fig. 4G, H). Meanwhile, we performed immunofluorescence analysis and nucleocytoplasmic separation examination and observed that the downregulation of G3BP1 in TSPYL5-overexpressing SK-N-SH cells decreased the nuclear export of p53 and that G3BP1 overexpression increased the nuclear export of p53 in TSPYL5-knockdown cells (Fig. 4I–L), indicating that the regulation of p53 cytoplasm translocation by TSPYL5 is dependent on the function of G3BP1.

Considering that G3BP1 acts as the core protein of stress granules (SGs) in cells under stress [33], we tested the involvement of SGs formation in TSPYL5/G3BP1-mediated p53 sumoylation. Treating cells with a frequently used SGs inducer arsenate, we clearly observed a cytoplasmic punctate pattern of G3BP1 (Supplementary Fig. 9a) and the increased phosphorylation of EIF2S1 (eukaryotic translation initiation factor 2 alpha at S51) (Supplementary Fig. 9b), a marker for showing SGs formation [34]. However, SGs formation did not interrupt the TSPYL5-increased p53 sumoylation and cytoplasmic location (Supplementary Fig. 9a, c). The interaction between TSPYL5 and G3BP1 were not reduced (Supplementary Fig. 9d), indicating that in cells with SGs, TSPYL5 still interacts with G3BP1 to activate G3BP1-mediated p53 sumoylation and nuclear export.

### TSPYL5/G3BP1-mediated p53 sumoylation requires RanBP2 involvement

Sumoylation, like ubiquitination, is also a sequential multienzymatic process in which SUMO E3 ligases play a critical role in the recruitment of substrates and the transfer of SUMOs onto targets [35]. To date, G3BP1 has not been demonstrated to function as an E3 ligase. Second, our work found that the binding of TSPYL5 to G3BP1 seriously disturbed the interaction between p53 and G3BP1 (Supplementary Fig. 10a, b), providing an explanation for the absence of the TSPYL5-G3BP1-p53 complex and suggesting that the binding of TSPYL5 to G3BP1 could not establish a functional platform for p53 sumoylation. In this case, we further explored the E3 sumo-ligases in G3BP1-interacting proteins by Co-IP and LC-MS/MS assays. The results indicated that RanBP2 was a high-scoring partner of G3BP1 (Fig. 5A). Previous studies have identified that RanBP2 is one of the E3 sumo-ligases for p53 sumoylation [36]. Therefore, we further performed IP and molecular docking assays and confirmed the binding between G3BP1 and RanBP2 in NB cells (Fig. 5B, C). More detailed work indicated that the PXXP domain (from 222 aa to 338 aa) of G3BP1 was necessary for its binding to RanBP2 (Fig. 5D).

Importantly, in the present study, we identified the presence of the RanBP2-G3BP1-p53 complex and the interaction among the three proteins in the complex (Fig. 5E), displaying a functional system potentially performing the sumoylation of p53. Furthermore, we observed that G3BP1 overexpression increased the binding between p53 and RanBP2 (Fig. 5F). Therefore, it is likely that in the RanBP2-G3BP1-p53 complex, G3BP1 acts as a recruiter of p53 to enhance the interaction between RanBP2 and p53 and promote RanBP2-mediated p53 sumoylation. Furthermore, downregulation of the E3 sumo-ligase RanBP2 promoted the nuclear translocation of p53 in SK-N-SH cells with different TSPYL5 levels (Fig. 5G), further supporting that RanBP2 is involved in TSPYL5-improved p53 sumoylation and nuclear export. Here, we are almost certain that G3BP1 and RanBP2 are two crucial members of the underlying mechanism of TSPYL5-regulated p53 sumoylation.



### TSPYL5 enhances the interaction of G3BP1 and RanBP2 by driving the nuclear membrane translocation of G3BP1

RanBP2 is a key component of the nuclear pore complex [37], but we did not observe a predominant distribution of either TSPYL5 or G3BP1 on the nuclear membrane of NB cells. This raises the question of how cytoplasmic TSPYL5 promotes the interaction of

RanBP2 and G3BP1 on the nuclear membrane. Encouragingly, we found that TSPYL5 overexpression promoted the translocation of G3BP1 to the nuclear membrane with colocalization with RanBP2 in SK-N-SH cells (Fig. 6A). Moreover, we observed that TSPYL5 overexpression enhanced the binding between G3BP1 and RanBP2 as well as the binding between RanBP2 and p53

**Fig. 4 TSPYL5-promoted p53 sumoylation depends on its interaction with G3BP1.** **A** Mass spectrometry analysis identified G3BP1 in the binding protein pool of TSPYL5. **B** Endogenous interaction between TSPYL5 and G3BP1 was determined using Co-IP with anti-TSPYL5 or anti-G3BP1 antibodies in SK-N-SH and SH-SY5Y cells. **C** Exogenous interaction between TSPYL5 and G3BP1 was determined using Co-IP with anti-HA or anti-MYC antibodies in SK-N-SH cells. **D** Interaction between the PXXP domain of G3BP1 and TSPYL5 was determined using Co-IP with anti-HA or anti-MYC antibodies. **E** The binding sites of TSPYL5 and G3BP1 proposed by computational docking model. TSPYL5 molecule was shown as blue sticks, and G3BP1 was shown as purple sticks. **F** G3BP1 promoted p53 sumoylation in SK-N-SH and SH-SY5Y cells. **G** The overexpression of G3BP1 increased the sumoylation level of p53 in SK-N-SH cells with TSPYL5 knockdown. **H** The knockdown of G3BP1 inhibited the positively effect of TSPYL5 on the sumoylation level of p53 in SK-N-SH cells. **I** Immunofluorescence analysis showed the increase of p53 nuclear translocation by the knockdown of G3BP1 in SK-N-SH cells with TSPYL5 overexpression. Scale bar = 20  $\mu$ m. **J** Nucleus-plasm separation examination showed the increase of p53 nuclear translocation by the knockdown of G3BP1 in SK-N-SH cells with TSPYL5 overexpression. **K** Immunofluorescence analysis showed the increase of p53 cytoplasm localization by the overexpression of G3BP1 in SK-N-SH cells with TSPYL5 knockdown. Scale bar = 20  $\mu$ m. **L** Nucleus-plasm separation examination assay showed the increase of p53 cytoplasm localization by the overexpression of G3BP1 in SK-N-SH cells with TSPYL5 knockdown.

(Fig. 6B, C). These findings reveal that TSPYL5 promotes the formation of the G3BP1/RanBP2/p53 complex by mediating the nuclear membrane accumulation of G3BP1. Nevertheless, we did not observe an interaction between TSPYL5 and RanBP2 or the presence of TSPYL5 in the RanBP2-G3BP1-p53 complex (Fig. 6D), although the binding of TSPYL5 to G3BP1 increased the formation of the RanBP2-G3BP1-p53 complex (Fig. 6E), and the PXXP domain of G3BP1 is necessary for binding to TSPYL5 or RanBP2. Thus, we speculate that TSPYL5 could be displaced by RanBP2 when G3BP1 interacts with RanBP2.

Furthermore, using human neuroblastoma tissues, we analyzed the correlation of the subcellular localization of p53 and G3BP1 with the expression level of TSPYL5. As a result, we observed clearly nuclear membrane aggregation of G3BP1 and cytoplasmic p53 sequestration in five cases of NB with abundant TSPYL5 expression, while such a phenotype of G3BP1 and p53 was absent in other three cases showing few TSPYL5 expression (Fig. 6F, Supplementary Fig. 11). These observations *in vivo* confirm a decisive role of high TSPYL5 expression in the nuclear membrane aggregation of G3BP1 and cytoplasmic p53 sequestration in NB tumors.

#### TSPYL5 promotes casein kinase 2-dependent G3BP1 Ser149 phosphorylation to drive G3BP1 translocation

To further investigate the mechanism of TSPYL5-driven nuclear membrane aggregation of G3BP1, we constructed fusion plasmids of each structural domain of G3BP1 fused with GFP (green fluorescent protein) (Fig. 7A). Firstly, we examined the subcellular location of G3BP1-GFP in the TSPYL5-knockdown cells. The results showed that the G3BP1-GFP proteins were dispersedly present in the cytoplasm of the TSPYL5-knockdown cells, with some locating around the nuclear periphery (Supplementary Fig. 12). Then, the immunofluorescence signal of G3BP1-GFP appeared to accumulate clearly in the nuclear periphery when TSPYL5 was overexpressed (Supplementary Fig. 12). These results indicated that TSPYL5 enhanced the aggregation of exogenous G3BP1 on the nuclear membrane.

Furthermore, the immunofluorescence analysis in SK-N-SH cells showed that regardless of whether TSPYL5 was overexpressed, PXXP domain-absent polypeptides containing the NTF2L (nuclear transport factor 2-like) domain were mainly localized in the nucleus; the polypeptides containing the NTF2L and PXXP domains showed nuclear membrane aggregation when overexpressing TSPYL5, while the polypeptides without the NTF2L domain were steadily present in the cytoplasm (Fig. 7B). Taken together, these findings suggest that both the NTF2L and PXXP domains of G3BP1 are indispensable for its nuclear membrane aggregation driven by TSPYL5.

The phosphorylation of G3BP1 at Ser149 in the NTF2L domain has been demonstrated to enhance the nuclear translocation of G3BP1 [38]. Undoubtedly, the nuclear import of G3BP1 could increase the chances of its RanBP2-binding retention on the nuclear membrane. Thus, we investigated the influence of the

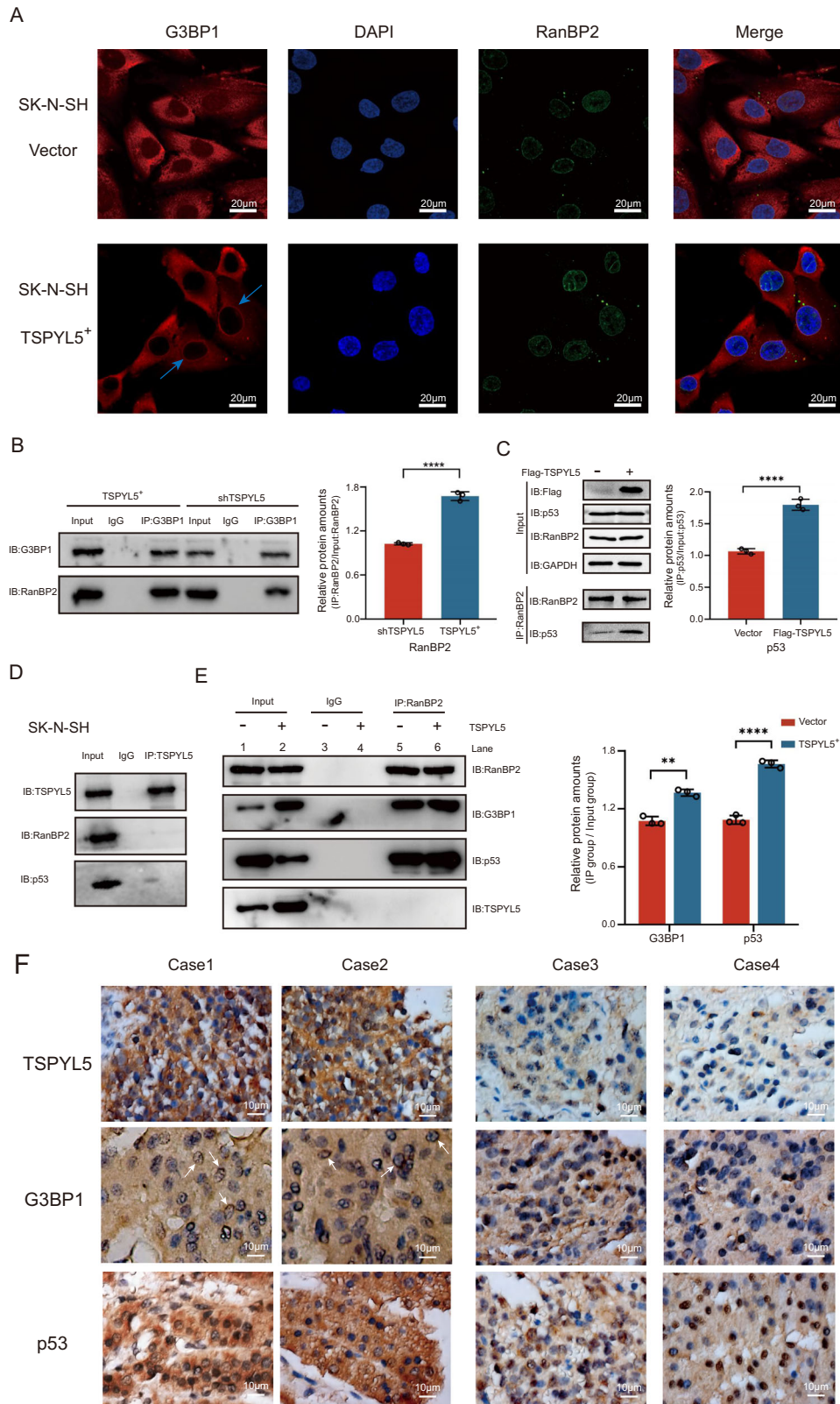
interaction of TSPYL5 with G3BP1 on G3BP1 phosphorylation. The results verified that TSPYL5 positively regulated G3BP1 Ser149 phosphorylation in NB cells (Fig. 7C), which was supported by the observation that the overexpression of TSPYL5 promoted G3BP1 phosphorylation (Fig. 7D). Moreover, we constructed vectors expressing GFP-fused G3BP1 mutants harboring Ser149Ala or Ser149Glu and observed that the mutations disturbed G3BP1 phosphorylation by TSPYL5 (Fig. 7E). Importantly, both mutants were mainly present in the cytoplasm regardless of whether TSPYL5 was overexpressed (Fig. 7F). Moreover, we treated cells with siRNA and chemical inhibitor TBB of casein kinase 2 (CK2) which has been demonstrated to phosphorylate G3BP1 at the site of Ser149 [39]. We found that the inhibition of CK2 activity decreased the levels of TSPYL5-mediated G3BP1 Ser149 phosphorylation (Fig. 7G), and p53 sumoylation followed (Fig. 7H). All of these results support that the interaction of TSPYL5 and G3BP1 promotes CK2-dependent G3BP1 Ser149 phosphorylation which further enhances the nuclear membrane translocation of G3BP1 to form the G3BP1/RanBP2/p53 complex for p53 sumoylation and nuclear export.

#### DISCUSSION

Our present study demonstrates a TSPYL5-driven molecular axis positively regulating p53 sumoylation and nuclear export, creating cytoplasmic p53 sequestration in NB cells (Fig. 8). In detail, TSPYL5 binding to the PXXP domain of G3BP1 enhances CK2-dependent G3BP1 Ser149 phosphorylation in the cytoplasm, promoting the NTF2L domain-dependent nuclear import of G3BP1; nucleoporin RanBP2 physically interacts with nuclear-transferred G3BP1, causing the aggregation of G3BP1 on the nuclear membrane; the binding of RanBP2 to G3BP1 dissociates TSPYL5 from G3BP1, recovering the ability of G3BP1 to bind to p53; G3BP1 recruits p53 for RanBP2 at the nuclear pore, facilitating the formation of the RanBP2-G3BP1-p53 complex; the increase in the RanBP2-G3BP1-p53 complex enhances RanBP2-mediated sumoylation of monoubiquitinated p53 in NB cells with low MDM2 levels, accelerating p53 nuclear export; the decrease in nuclear p53 suppresses its transcriptional activity and further lowers MDM2 levels, positively feeding back for p53 monoubiquitination/sumoylation-mediated nuclear export and cytoplasm localization. Our findings uncovered a dynamic model regulating p53 sumoylation, proposing the mechanism underlying p53 cytoplasm sequestration in NB. The suppression of p53 nuclear function by TSPYL5/G3BP1 could provide additional clues for the etiology and treatment of NB cancers, considering the remarkable anti-cancer effect of wild-type p53. Similarly, we suggest that it is of significance to explore whether the TSPYL5-driven mechanism works in other cancers with preponderant cytoplasm localization of p53 and abundant ectopic expression of TSPYL5, including part of breast, liver, and colorectal cancers [40].

Similar to ubiquitination, sumoylation requires E3 ligases to recruit substrates and accelerate the transfer of SUMOs onto





TSPYL5 as a novel risk factor for NB classification to intensify postoperative treatment and improve the prognosis of patients with high TSPYL5 expression. Additionally, we must acknowledge that the limitations that exist in the present study. Firstly, we could not obtain the fresh neuroblastoma tissues in which to investigate the

nuclear periphery location of G3BP1 and its interaction with TSPYL5. Secondly, we failed to obtain the tumor-bearing mice using the subcutaneous injection of SK-N-SH or SH-SY5Y cells in BALB/c nude mice, as a result, we did not examine the potential role of TSPYL5 in an in vivo mouse model of NB. Despite all this, the recent patient-

**Fig. 6 TSPYL5 enhances the nuclear membrane aggregation of G3BP1 to facilitate the formation of RanBP2-G3BP1-p53 complex.** **A** Immunofluorescence analysis showed the increase of G3BP1 on the nuclear membrane in SK-N-SH with TSPYL5 overexpression (blue arrows pointed). Scale bar = 20  $\mu$ m. **B** TSPYL5 overexpression increased the binding of G3BP1 to RanBP2. Nuclear proteins are isolated for Co-IP. Data are presented as the mean  $\pm$  SD from three experiments, \*\*\* $p$  < 0.001. **C** TSPYL5 overexpression increased the binding of RanBP2 to p53. Data are presented as the mean  $\pm$  SD from three experiments, \*\*\* $p$  < 0.001. **D** Co-IP assays showed the absence of TSPYL5-RanBP2 or TSPYL5-p53 complexes in SK-N-SH cells. Nuclear proteins are isolated for Co-IP. **E** Co-IP assays with nucleoproteins showed the increase of the binding of RanBP2 and G3BP1 or p53 in SK-N-SH with TSPYL5 overexpression. **F** Immunohistochemistry assays showed nuclear membrane aggregation of G3BP1 and cytoplasmic p53 sequestration in two cases with abundant TSPYL5 expression (case 1 and case 2), and such a phenotype of G3BP1 and p53 was absent in other two cases showing few TSPYL5 expression (case 3 and case 4). White arrows indicated the nuclear membrane location of G3BP1. Scale bar = 10  $\mu$ m.

derived organoid/xenograft models, acting as advanced tools, will be useful to further explore the biological functions and clinical significance of TSPYL5 in NB.

In conclusion, our study reveals that TSPYL5 uniquely suppresses p53 signaling by promoting G3BP1/RanBP2-mediated p53 sumoylation to tether p53 in the cytoplasm of NB cells. We demonstrate that the abundant ectopic expression of TSPYL5 is not conducive to NB treatment and prognosis, suggesting that the depletion of TSPYL5 and disruption of the interaction between TSPYL5 and G3BP1 may provide interesting therapeutic opportunities for NB patients.

## MATERIALS AND METHODS

### Cell culture

All cell lines used in this study were purchased from the Type Culture Collection of the Chinese Academy of Sciences (Shanghai, China) and maintained in our laboratory. SK-N-SH and SH-SY5Y cells were cultured in Minimum Essential Medium (HyClone, Logan, UT) containing 1% penicillin/streptomycin (HyClone), 10% fetal bovine serum (FBS) (Gibco, Carlsbad, CA), 1% nonessential amino acids (Procell, Wuhan, China), and 1% sodium pyruvate (Procell). Other cells were grown in RPMI-1640 (HyClone) medium supplemented with 10% FBS and 1% penicillin/streptomycin. Cells were incubated at 37 °C in a humid atmosphere with 5% CO<sub>2</sub> and 95% air.

### Chemicals and antibodies

All chemicals for the experiments were reagent grade or better. The protease inhibitor, MG132, was provided by Selleck (Billerica, MA). Cisplatin and 4,5,6,7-tetrabromobenzotriazole (TBB) were obtained from MedChem-Express (MCE, Shanghai, China). Verapamil and Hoechst 33342 were purchased from Solarbio (Beijing, China). Arsenate was provided by Sigma-Aldrich (St. Louis, MO). Details of the specific antibodies used in this study are listed in Supplementary Table 1.

### DNA constructs and mutagenesis

The cDNA of *TSPYL5*, *G3BP1*, *TP53*, and *SUMO1* were separately synthesized and cloned and inserted into a pcDNA<sup>TM</sup>3.1(+) vector (Invitrogen, Carlsbad, CA) containing a tag sequence of FLAG, HA or Myc. Three lentiviral vectors for overexpressing, knocking down, and recovering TSPYL5 expression were constructed by GeneCopia (Rockville, MD). Additionally, the full-length cDNA of *TSPYL5* was also cloned and inserted into a pLVX-ZsGreen1-N1 vector (GeneCopia). *TSPYL5*-specific shRNA (shTSPYL5) was synthesized and inserted into the pLKO.1 vector (GeneCopia). All siRNAs used in this study were synthesized by GenePharma Co., Ltd. (Shanghai, China). The sequences of the siRNAs are listed in Supplementary Table 2. Three mutant expression vectors, including p53-K386R, G3BP1-S149A, and G3BP1-S149E, were generated by PANOMIX Biomedical Tech Co., LTD (Suzhou, China).

### Immunoprecipitation (IP) and western blotting

Cells were lysed with lysis buffer containing protease inhibitor cocktail (Bimake, Carlsbad, CA) and phosphatase inhibitor cocktail (Bimake), followed by centrifugation at 4 °C. The supernatants were immunoprecipitated with the indicated antibodies or IgG and incubated overnight at 4 °C. Then, the mixture was additionally incubated with Protein A+G Agarose beads (Beyotime, Shanghai, China) and rotated for 2 h at 4 °C. After washing five times with lysis buffer, the beads were mixed with SDS-PAGE loading buffer and boiled for 8 min. After separation by SDS-PAGE, the proteins were transferred onto polyvinylidene difluoride membranes (Millipore, Billerica, MA). Following the blocking procedure, membranes were reacted with

primary antibodies overnight at 4 °C. The membranes were washed three times and incubated with secondary antibodies for 2 h at room temperature. Specific proteins were visualized using an Immobilon<sup>TM</sup> chemiluminescence western blotting detection system (Millipore).

### Liquid chromatography-tandem mass spectrometry (LC-MS/MS)

IP samples were separated by SDS-PAGE, and protein bands were excised from the gel. These protein fragments were washed twice with 100 mM bicarbonate in acetonitrile and then digested with trypsin. Then, 0.1% formic acid was added to the supernatants, which were subjected to LC-MS/MS analysis with an Orbitrap-Fusion mass spectrometer (Thermo Scientific, Waltham, MA) accompanied by Easy-nLC 1000 (Thermo Scientific). Datasets were generated from at least three independent experiments. The raw data derived from the LC-MS/MS analysis were used in Proteome Discoverer 2.4 (Thermo Scientific).

### Transcriptomic analysis

Total RNA was isolated using TRIzol reagent (Invitrogen). After determining the quality and concentration using an Agilent 2100 bioanalyzer (Agilent Technologies, Santa Clara, CA), RNAs were reverse transcribed and sequenced in a HiSeq6000 instrument (Illumina, San Diego, CA). Triplicate RNA samples of each group were prepared for sequencing. The bioinformatic analysis was carried out by Genedenovo Biotechnology Company (Guangzhou, China). Gene Ontology (GO) analysis was visualized for annotation, visualization, and integrated discovery by using the database (<https://david.ncicrf.gov/>). GeneRatio was calculated by the percentage of differentially expressed genes (DEGs) that matched a specific GO term in the total DEGs. Kyoto Encyclopedia of Genes and Genomes (KEGG) pathway enrichment analysis was performed by using the KEGG Orthology-based Annotation System 2.0 (KOBAS 2.0, <http://kobas.cbi.pku.edu.cn>).

### Single-cell RNA-seq data reanalysis

The single-cell RNA-seq data of 14 patients with NB were obtained from the GEO (GSE137804) database, and the clinical characteristics of the samples were collected from the report [17]. After removing cells with a gene count of 500–6000, a unique molecular identifier (UMI) below 30,000, or more than 20% mitochondrial content, a total of 164,296 cells were used for subsequent analyses. Seurat v2.3 was used for dimension reduction and clustering. NormalizeData and ScaleData were used to normalize and scale all gene expression values. The top 2,000 variable genes were selected for principal component analysis (PCA) by FindVariableFeatures. Using the top 20 principal components and a resolution parameter of 0.5, the cells were separated into six clusters by the FindClusters function. For two-dimensional visualization, the RunUMAP function generated uniform manifold approximation and projection (UMAP) plots by the same PCs (principal components) and default settings.

### Reverse transcription-quantitative PCR (RT-qPCR)

Total RNA was reverse transcribed into cDNA using a RevertAid First-Strand cDNA Synthesis Kit (Thermo Scientific). Using SYBR Green Master Mix, quantitative PCR was performed in an iCycler IQ<sup>TM</sup> system (Bio-Rad, Hercules, CA). Each assay was carried out in triplicate. *GAPDH* was used as an internal control. The RT-qPCR primers for target genes are listed in Supplementary Table 3.

### Cell proliferation, invasion, and migration assays

For cell proliferation assays, cells were seeded into a 96-well plate (3000 cells/well) and incubated overnight. The next day, cells were treated with 10  $\mu$ M

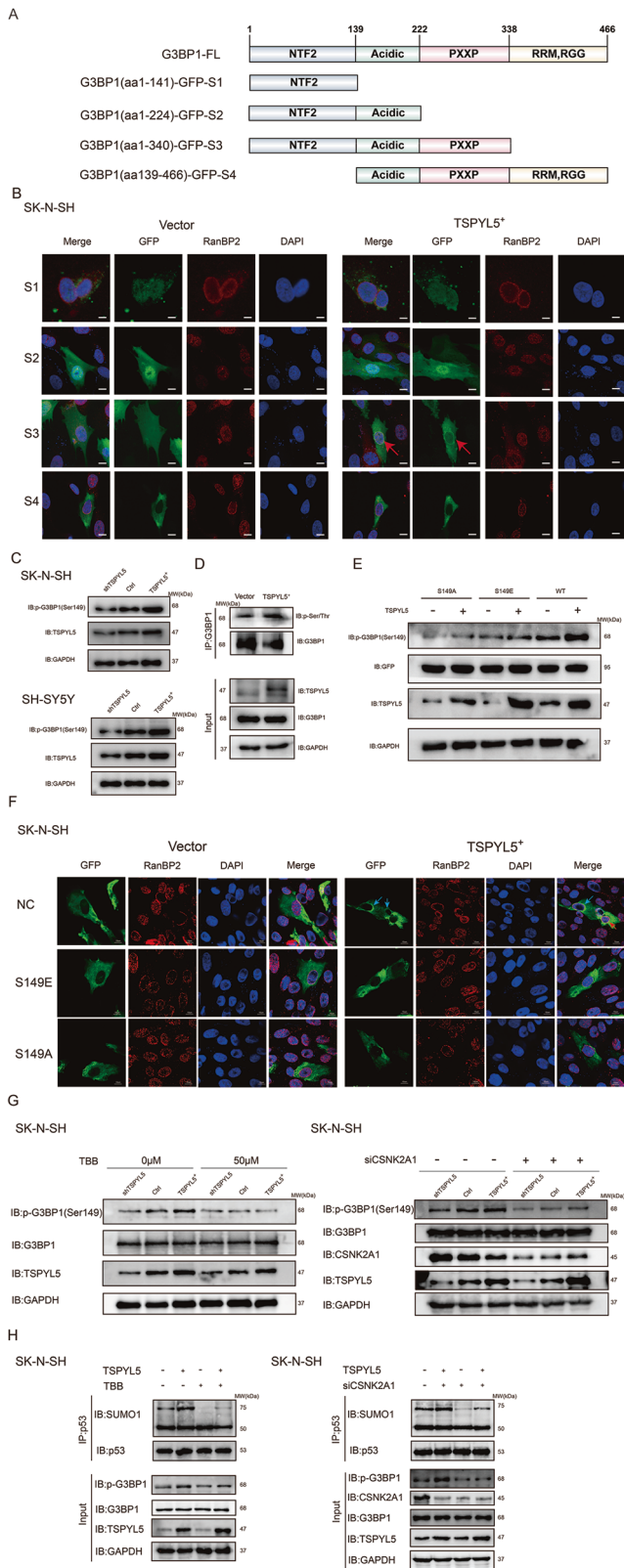


**Fig. 7 TSPYL5 promotes the phosphorylation of G3BP1 Ser149 to facilitate its nuclear membrane translocation.** **A** Schematic diagram of G3BP1 domain and GFP-fused proteins. **B** Immunofluorescence analysis showed the subcellular location of each fused protein in SK-N-SH cells with TSPYL5 overexpression. Red arrows indicated the nuclear membrane location of the fused proteins. Scale bar = 20  $\mu\text{m}$ . **C** Western blotting with specific antibody of anti-phosphorylated Ser149 of G3BP1 showed the increase in the level of G3BP1 Ser149 phosphorylation in SK-N-SH cells with TSPYL5 overexpression. **D** Co-IP assay showed the increase in the total level of G3BP1 phosphorylation in SK-N-SH cells with TSPYL5 overexpression. **E** The promotion of G3BP1 phosphorylation was absent in TSPYL5-overexpressed SK-N-SH cells with S149A or S149E mutant. **F** The promotion of the nuclear membrane aggregation of G3BP1 was absent in TSPYL5-overexpressed SK-N-SH cells with S149A or S149E mutant. Scale bar = 10  $\mu\text{m}$ . **G** The inhibition of CK2 activity via TBB or CSNK2A1 siRNA decreased the phosphorylation levels of G3BP1 Ser149, even TSPYL5 overexpression. **H** The sumoylated p53 levels declined when inhibiting CK2 activity via TBB or CSNK2A1 siRNA, even TSPYL5 overexpression.

### Colony formation assay

Cells were seeded into 35-mm plates with a density of 1000 cells per well for colony formation assay. After culturing for 10–14 days, cells were washed by PBS, fixed with formaldehyde, and stained with 0.5% crystal violet (Biosharp, Shanghai, China) for 30 min at room temperature. Colonies with more than 50 cells were counted manually and photographed.

### Sphere formation assay

Cells were cultured in stem cell-permissive medium (Gibco), containing epidermal growth factor (20 ng/mL), basic fibroblast growth factor (20 ng/mL), and B27 serum-free supplement. Suspended cells were seeded into ultralow-attachment 96-well plates (Jet Bio-Filtration, Guangzhou, China) at a density of 1 or 2 cells/well and incubated at 37  $^{\circ}\text{C}$  for 24 h. Then, each well was visually checked for the presence of a single cell. After 10–14 days, spheres were quantitated and photographed under an Olympus IX71 fluorescent microscopy (Olympus, Tokyo, Japan).

### Flow cytometry assay

For cell apoptosis analysis, cells were seeded in 6-well plates in MEM medium with 10% FBS for 24 h and treated with cisplatin. Apoptosis of cells was assessed according to the instructions of the Annexin V-Alexa Fluor 647/PI apoptosis detection kit (BD Pharmacy). Apoptotic cells were identified as both annexin V<sup>+</sup>/PI<sup>-</sup> and annexin V<sup>+</sup>/PI<sup>+</sup>.

For side population assay, cells were harvested and resuspended at a concentration of  $1 \times 10^5$  cells/ml and then given 75  $\mu\text{M}$  verapamil (Sigma-Aldrich) for 30 min. The DNA binding dye, Hoechst 33342 (Sigma-Aldrich), was then added to a final concentration of 5  $\mu\text{g}/\text{ml}$  and incubated for 90 min in the dark with interval mixing. Cells were then resuspended in ice-cold Hank's balanced salt solution. PI was added 10 min before sorting to a final concentration of 2  $\mu\text{g}/\text{ml}$ .

### Immunofluorescence staining and confocal imaging

For immunofluorescence analysis, cells were cultured on circular coverslips (Biosharp) in 24-well plates, fixed with 4% paraformaldehyde for 15 min, permeabilized with 0.1% Triton X-100 in phosphate-buffered saline (PBS) for 10 min, and incubated with 1% BSA for 1 h at room temperature. Following incubation with primary antibodies at 4  $^{\circ}\text{C}$  overnight, the cells were washed three times with PBS and incubated with Alexa Fluor 488-/555-/647-labeled secondary antibodies (Thermo Scientific). 4',6-diamidino-2-phenylindole (DAPI, Solarbio) was used for nuclear staining. Images were visualized by an orthostatic two-photon confocal microscope (Nikon, Tokyo, Japan).  $\alpha$ -Tubulin, RanBP2, and DAPI (4',6-diamidino-2-phenylindole) are used separately as the markers of cytoplasm, nuclear membrane, and nucleus in cells.

### Immunohistochemistry

A tissue microarray containing 22 NB specimens was obtained from Bioitech (Xian, China). The slide was deparaffinized, rehydrated, blocked with 3%  $\text{H}_2\text{O}_2$ , and separately incubated with primary antibodies, including anti-TSPYL5, anti-G3BP1, and anti-p53. After washing in PBS, slides were

cisplatin. Using the Cell Counting Kit-8 (Vazyme, Nanjing, China), cell numbers were measured every 24 h four times. Cell invasion assays were performed with Matrigel-coated chambers (BD Biosciences, Franklin Lakes, NJ). After staining, cells were counted using a light microscope in four randomly selected fields. Cell migration was examined by using wound healing migration assays. The migration areas were calculated using Prism 8 software.

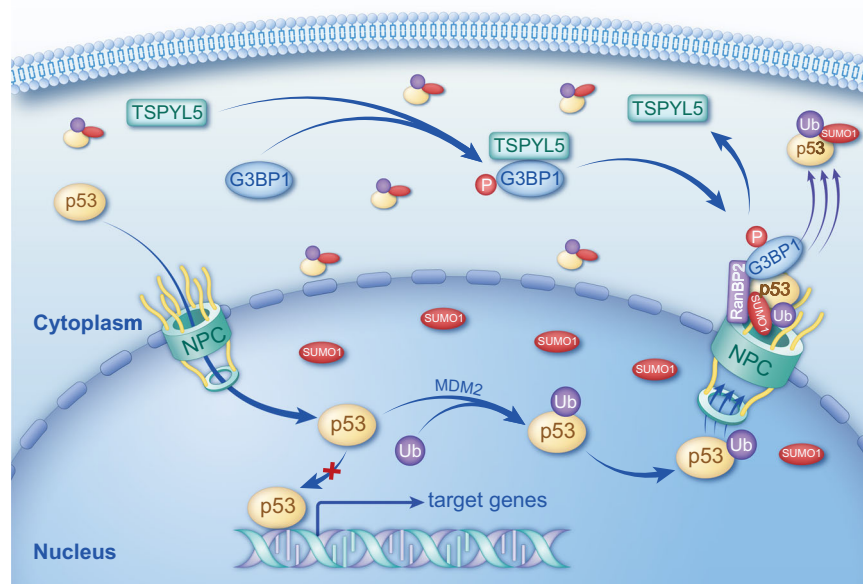


**Fig. 8** Proposed model of TSPYL5-driven nuclear membrane aggregation of G3BP1 and RanBP2/SUMO1-mediated p53 cytoplasm sequestration in neuroblastoma cells.

incubated in horseradish peroxidase-conjugated goat anti-rabbit IgG (Proteintech, Wuhan, China) followed by incubation with 3,3'-diaminobenzidine (DAB) substrate (AbsinBioscience, Shanghai, China) and counterstaining with hematoxylin solution. Preimmune rabbit serum was used as a negative control for primary antibodies. The slides were examined under a microscope (AX10 imager, Zeiss, Oberkochen, Germany). Among the 22 NB specimens, only eight were observed the signals of TSPYL5, G3BP1, and p53, simultaneously, while the complete signals of the three proteins could not be obtained in other specimens due to the destruction of their tissues.

### Statistical analysis

GraphPad Prism 8 software was used for statistical analysis. All data from at least three independent experiments are expressed as the mean  $\pm$  SD. Statistical significance between any two groups was tested using Student's *t*-test.  $P < 0.05$  was considered statistically significant.

### DATA AVAILABILITY

RNA sequencing data have been deposited to the Gene Expression Omnibus (GEO) and can be accessed using the following identifiers: GSE223866. Other single-cell RNA sequencing data used in this study are publicly available and can be accessed from GEO for the GSE137804. Additional data related to this paper may be requested from the corresponding author.

### REFERENCES

- Kamihara J, Bourdeaut F, Foulkes WD, Molenaar JJ, Mossé YP, Nakagawara A, et al. Retinoblastoma and neuroblastoma predisposition and surveillance. *Clin Cancer Res.* 2017;23:e98–106.
- Bahmad HF, Chamaa F, Assi S, Chalhoub RM, Abou-Antoun T, Abou-Kheir W. Cancer stem cells in neuroblastoma: expanding the therapeutic frontier. *Front Mol Neurosci.* 2019;12:131.
- Spike BT, Wahl GM. p53, Stem cells, and reprogramming: tumor suppression beyond guarding the genome. *Genes Cancer.* 2011;2:404–19.
- Chiche A, Moumen M, Romagnoli M, Petit V, Lasla H, Jézéquel P, et al. p53 deficiency induces cancer stem cell pool expansion in a mouse model of triple-negative breast tumors. *Oncogene.* 2017;36:2355–65.
- Chiche A, Moumen M, Petit V, Jonkers J, Medina D, Deugnier MA, et al. Somatic loss of p53 leads to stem/progenitor cell amplification in both mammary epithelial compartments, basal and luminal. *Stem Cells.* 2013;31:1857–67.
- Goldman SC, Chen CY, Lansing TJ, Gilmer TM, Kastan MB. The p53 signal transduction pathway is intact in human neuroblastoma despite cytoplasmic localization. *Am J Pathol.* 1996;148:1381–5.
- Oh L, Hafsi H, Hainaut P, Ariffin H. p53, stem cell biology and childhood blastomas. *Curr Opin Oncol.* 2019;31:84–91.
- Ostermeyer AG, Runko E, Winkfield B, Ahn B, Moll UM. Cytoplasmically sequestered wild-type p53 protein in neuroblastoma is relocated to the nucleus by a C-terminal peptide. *Proc Natl Acad Sci USA.* 1996;93:15190–4.
- Mitra S, Muralidharan SV, Di Marco M, Juvvuna PK, Kosalai ST, Reischl S, et al. Subcellular distribution of p53 by the p53-responsive lncRNA NBAT1 determines chemotherapeutic response in neuroblastoma. *Cancer Res.* 2021;81:1457–71.
- Carter S, Bischof O, Dejean A, Vousden KH. C-terminal modifications regulate MDM2 dissociation and nuclear export of p53. *Nat Cell Biol.* 2007;9:428–35.
- Santiago A, Li D, Zhao LY, Godsey A, Liao D. p53 SUMOylation promotes its nuclear export by facilitating its release from the nuclear export receptor CRM1. *Mol Biol Cell.* 2013;24:2739–52.
- Epping MT, Meijer LA, Krijgsman O, Bos JL, Pandolfi PP, Bernards R. TSPYL5 suppresses p53 levels and function by physical interaction with USP7. *Nat Cell Biol.* 2011;13:102–8.
- Kim IG, Lee JH, Kim SY, Heo CK, Kim RK, Cho EW. Targeting therapy-resistant lung cancer stem cells via disruption of the AKT/TSPYL5/PTEEN positive-feedback loop. *Commun Biol.* 2021;4:778.
- Fan L, Li H, Zhang Y. LINC00908 negatively regulates microRNA-483-5p to increase TSPYL5 expression and inhibit the development of prostate cancer. *Cancer Cell Int.* 2020;20:10.
- Na HJ, Yeum CE, Kim HS, Lee J, Kim JY, Cho YS. TSPYL5-mediated inhibition of p53 promotes human endothelial cell function. *Angiogenesis.* 2019;22:281–93.
- Episkopou H, Diman A, Claude E, Viceconte N, Decottignies A. TSPYL5 depletion induces specific death of ALT cells through USP7-dependent proteasomal degradation of POT1. *Mol Cell.* 2019;75:469–82.
- Dong R, Yang R, Zhan Y, Lai HD, Ye CJ, Yao XY, et al. Single-cell characterization of malignant phenotypes and developmental trajectories of adrenal neuroblastoma. *Cancer Cell.* 2020;38:716–33.
- Klusmann I, Rodewald S, Müller L, Friedrich M, Wienken M, Li Y, et al. p53 Activity results in DNA replication fork processivity. *Cell Rep.* 2016;17:1845–57.
- Wu C, Cui Y, Liu X, Zhang F, Lu LY, Yu X. The RNF20/40 complex regulates p53-dependent gene transcription and mRNA splicing. *J Mol Cell Biol.* 2020;12:113–24.
- Golubovskaya VM, Cance W. Focal adhesion kinase and p53 signal transduction pathways in cancer. *Front Biosci.* 2010;15:901–12.
- Wang Z, Strasser A, Kelly GL. Should mutant TP53 be targeted for cancer therapy?. *Cell Death Differ.* 2022;29:911–20.
- Levine AJ. p53: 800 million years of evolution and 40 years of discovery. *Nat Rev Cancer.* 2020;20:471–80.
- Stracquadanio G, Wang X, Wallace MD, Grawenda AM, Zhang P, Hewitt J, et al. The importance of p53 pathway genetics in inherited and somatic cancer genomes. *Nat Rev Cancer.* 2016;16:251–65.
- Li M, Knight DA, Smyth MJ, Stewart TJ. Sensitivity of a novel model of mammary cancer stem cell-like cells to TNF-related death pathways. *Cancer Immunol Immunother.* 2012;61:1255–68.

25. Engeland K. Cell cycle arrest through indirect transcriptional repression by p53: I have a DREAM. *Cell Death Differ.* 2018;25:114–32.
26. Vaddavalli PL, Schumacher B. The p53 network: cellular and systemic DNA damage responses in cancer and aging. *Trends Genet.* 2022;38:598–612.
27. Tweddle DA, Pearson AD, Haber M, Norris MD, Xue C, Flemming C, et al. The p53 pathway and its inactivation in neuroblastoma. *Cancer Lett.* 2003;197:93–8.
28. Li M, Brooks CL, Wu-Baer F, Chen D, Baer R, Gu W. Mono- versus polyubiquitination: differential control of p53 fate by Mdm2. *Science.* 2003;302:1972–5.
29. Feng YC, Liu XY, Teng L, Ji Q, Wu Y, Li JM, et al. c-Myc inactivation of p53 through the pan-cancer lncRNA MILIP drives cancer pathogenesis. *Nat Commun.* 2020;11:4980.
30. Kwek SS, Derry J, Tyner AL, Shen Z, Gudkov AV. Functional analysis and intracellular localization of p53 modified by SUMO-1. *Oncogene.* 2001;20:2587–99.
31. Becker K, Marchenko ND, Maurice M, Moll UM. Hyperubiquitylation of wild-type p53 contributes to cytoplasmic sequestration in neuroblastoma. *Cell Death Differ.* 2007;14:1350–60.
32. Mao C, Wang X, Liu Y, Wang M, Yan B, Jiang Y, et al. A G3BP1-interacting lncRNA promotes ferroptosis and apoptosis in cancer via nuclear sequestration of p53. *Cancer Res.* 2018;78:3484–96.
33. Yang P, Mathieu C, Kolaitis RM, Zhang P, Messing J, Yurtsever U, et al. G3BP1 is a tunable switch that triggers phase separation to assemble stress granules. *Cell.* 2020;181:325–45.
34. Prentzell MT, Rehbein U, Cadena Sandoval M, De Meulemeester AS, Baumeister R, Brohé L, et al. G3BPs tether the TSC complex to lysosomes and suppress mTORC1 signaling. *Cell.* 2021;184:655–74.
35. Chang HM, Yeh ETH. SUMO: from bench to bedside. *Physiol Rev.* 2020;100:1599–619.
36. Blondel-Tepaz E, Leverage M, Sokrat B, Paradis JS, Kopic M, Saha K, et al. The RanBP2/RanGAP1-SUMO complex gates  $\beta$ -arrestin2 nuclear entry to regulate the Mdm2-p53 signaling axis. *Oncogene.* 2021;40:2243–57.
37. Ritterhoff T, Das H, Hofhaus G, Schröder RR, Flotho A, Melchior F. The RanBP2/RanGAP1\*SUMO1/Ubc9 SUMO E3 ligase is a disassembly machine for Crm1-dependent nuclear export complexes. *Nat Commun.* 2016;7:11482.
38. Tourrière H, Gallouzi IE, Chebli K, Capony JP, Mouaikel J, van der Geer P, et al. RasGAP-associated endoribonuclease G3BP: selective RNA degradation and phosphorylation-dependent localization. *Mol Cell Biol.* 2001;21:7747–60.
39. Sahoo PK, Kar AN, Samra N, Terenzio M, Patel P, Lee SJ, et al. A Ca<sup>2+</sup>-dependent switch activates axonal casein kinase 2 $\alpha$  translation and drives G3BP1 granule disassembly for axon regeneration. *Curr Biol.* 2020;30:4882–95.
40. Fojo T. p53 as a therapeutic target: unresolved issues on the road to cancer therapy targeting mutant p53. *Drug Resist Updates.* 2002;5:209–16.
41. Shi X, Du Y, Li S, Wu H. The role of SUMO E3 ligases in signaling pathway of cancer cells. *Int J Mol Sci.* 2022;23:3639.
42. Pichler A, Knipscheer P, Saitoh H, Sixma TK, Melchior F. The RanBP2 SUMO E3 ligase is neither HECT- nor RING-type. *Nat Struct Mol Biol.* 2004;11:984–91.
43. Ashikari D, Takayama K, Tanaka T, Suzuki Y, Obinata D, Fujimura T, et al. Androgen induces G3BP2 and SUMO-mediated p53 nuclear export in prostate cancer. *Oncogene.* 2017;36:6272–81.
44. Takayama KI, Suzuki T, Tanaka T, Fujimura T, Takahashi S, Urano T, et al. TRIM25 enhances cell growth and cell survival by modulating p53 signals via interaction with G3BP2 in prostate cancer. *Oncogene.* 2018;37:2165–80.
45. Irwin MS, Naranjo A, Zhang FF, Cohn SL, London WB, Gastier-Foster JM, et al. Revised neuroblastoma risk classification system: a report from the Children's Oncology Group. *J Clin Oncol.* 2021;39:3229–41.
46. Zafar A, Wang W, Liu G, Wang X, Xian W, McKeon F, et al. Molecular targeting therapies for neuroblastoma: progress and challenges. *Med Res Rev.* 2021;41:961–1021.
47. Cheung NK, Dyer MA. Neuroblastoma: developmental biology, cancer genomics and immunotherapy. *Nat Rev Cancer.* 2013;13:397–411.
48. Chen L, Malcolm AJ, Wood KM, Cole M, Variend S, Cullinane C, et al. p53 is nuclear and functional in both undifferentiated and differentiated neuroblastoma. *Cell Cycle.* 2007;6:2685–96.
49. Moll UM, Ostermeyer AG, Haladay R, Winkfield B, Frazier M, Zambetti G. Cytoplasmic sequestration of wild-type p53 protein impairs the G1 checkpoint after DNA damage. *Mol Cell Biol.* 1996;16:1126–37.
50. Van Maerken T, Speleman F, Vermeulen J, Lambertz I, De Clercq S, De Smet E, et al. Small-molecule MDM2 antagonists as a new therapy concept for neuroblastoma. *Cancer Res.* 2006;66:9646–55.
51. Shen H, Maki CG. Pharmacologic activation of p53 by small-molecule MDM2 antagonists. *Curr Pharm Des.* 2011;17:560–8.
52. Soragni A, Janzen DM, Johnson LM, Lindgren AG, Thai-Quynh Nguyen A, Tiourin E, et al. A designed inhibitor of p53 aggregation rescues p53 tumor suppression in ovarian carcinomas. *Cancer Cell.* 2016;29:90–103.
53. Iwahashi N, Ikezaki M, Komohara Y, Fujiwara Y, Noguchi T, Nishioka K, et al. Cytoplasmic p53 aggregates accumulated in p53-mutated cancer correlate with poor prognosis. *PNAS Nexus.* 2022;1:pgac128.

## ACKNOWLEDGEMENTS

We thank the staff of the Research Core Facility and the Laboratory of Pathology, West China Hospital, Sichuan University, China, for their assistance in instrument operation and their support for the immunohistochemistry examination. We appreciate all the patients who are enrolled in this study.

## AUTHOR CONTRIBUTIONS

YY and YQL designed and supervised the research project. ZKW and YWZ performed the wet laboratory work. YY, YQL, ZKW, YWZ, JYS, SYX, MY, and XYZ analyzed and interpreted the data. DCT provided the technical and/or material support. YQL and ZKW drafted the manuscript. YY and YQL revised the manuscript. All authors edited and approved the final version of the manuscript.

## FUNDING

This study was supported by Grant 81871203 (Yuan Yang) from the National Natural Science Foundation of China.

## COMPETING INTERESTS

The authors declare no competing interests.

## ETHICS APPROVAL

This study was approved by the Ethics Committee of West China Hospital in Sichuan University (Ethics No.: 2018026a). All methods were performed in accordance with the relevant guidelines and regulations. The informed consent for neuroblastoma tissues was obtained from the patients or their legal guardians.

## ADDITIONAL INFORMATION

**Supplementary information** The online version contains supplementary material available at <https://doi.org/10.1038/s41419-025-07694-x>.

**Correspondence** and requests for materials should be addressed to Yuan Yang.

**Reprints and permission information** is available at <http://www.nature.com/reprints>

**Publisher's note** Springer Nature remains neutral with regard to jurisdictional claims in published maps and institutional affiliations.



**Open Access** This article is licensed under a Creative Commons Attribution 4.0 International License, which permits use, sharing, adaptation, distribution and reproduction in any medium or format, as long as you give appropriate credit to the original author(s) and the source, provide a link to the Creative Commons licence, and indicate if changes were made. The images or other third party material in this article are included in the article's Creative Commons licence, unless indicated otherwise in a credit line to the material. If material is not included in the article's Creative Commons licence and your intended use is not permitted by statutory regulation or exceeds the permitted use, you will need to obtain permission directly from the copyright holder. To view a copy of this licence, visit <http://creativecommons.org/licenses/by/4.0/>.

© The Author(s) 2025